JOURNAL OF MATERIALS SCIENCE 25 (1990) 3714–3722

Adhesion of lacquer to phosphated steel – a shear test evaluation

Y. M. ARAVOT*, LELIA ARCAN*, M. E. ARCAN‡, ANA ALBU-YARON*
*ARO, The Volcani Center, P.O.B. 6, Bet Dagan 50250, Israel
‡Tel-Aviv University, Tel Aviv 69978, Israel

Measurement of the adhesion toughness of a fast cure thermosetting powder coating used for corrosion protection of cold-rolled steel has been attempted in a shear test under uniform plane stress loading conditions at the interface. A specially designed test specimen preparation procedure (by direct crosslinking) and geometry (symmetrical) was developed to enable proper mechanical behaviour under shear initiation of fracture and uniform plane stress loading in the significant section of the specimen – the interface. The shear test was designed to measure the nominal and the net ultimate shear stress values $(USS)_n$ and $(USS)_{net}$, as well as the critical stress intensity factor (SIF) of interfaces. From experimentally measured critical load at which the adhesion failed, the ultimate shear stress values (USS_{net} $N\,mm^{-2}$) were calculated and used as a quantitative information of the bond toughness along the interfaces. The experimental results with a range of specimens revealed that the test can, indeed, discern subtle variations influencing adhesion such as type of cold-rolled steel, an iron phosphate pretreatment before coating or variation in stoving temperatures. Fractographic analysis of shear failed specimens on mating surfaces revealed generation of a microcrack network in most of the fracture pattern tested, indicating fracture mechanism transitions characteristic of pure shear for both iron phosphated free cold-rolled steel–lacquer (SL) as well as for iron phosphated cold-rolled steel–lacquer (SPL) specimens. The fractographs, however, indicate fracture propagation more difficult for SPL specimens and comparatively smooth fracture surface for SL specimens, obviously affected by variations in their respective interface structure and morphology. This behaviour correlates well with measurements of $(USS)_{net}$ in test.

1. Introduction

Coatings are applied to a substrate in order to change certain parts of its characteristics, e.g. corrosion protection, anti-reflection, improvement of surface hardness, etc. By definition, they require perfection in adhesion. If the adhesion is poor, the extent of deterioration of the substrate by environmental factors is greatly accelerated, with loss of adhesion as the extreme interfacial failure.

As the interfacial failure is the dominant mechanism limiting the reliability of such a system, much research has been undertaken to understand the complex physics, chemistry and mechanics associated with adhesion [1–4] as well as to develop a reliable, reproducible and quantitative method for measuring the strength of the interfacial adhesion which actually affects the system.

Despite the large amount of research devoted to the development of various types of adhesion testing, the adhesion measurement methods available in industry, like the scratch test, the wedge method and the attached traction piece test, all entail specific limitations which depend on the load capacity, the strength of the bonding method and the character of the individual transfer devices. It must be added also that they present the common limitations of the direct linkage to the coating surface of the mechanically attached traction piece in test. This is accomplished with a bonding agent, used in direct contact with the coating surface, which introduces undue stress on binding (when drying, for example) to the film and which risks reacting chemically with the coating, thus changing its true character. All those limitations cause errors in results.

In an effort to obtain quantitative information about lacquer bonding on cold-rolled steel (SL) and on phosphated cold-rolled steel (SPL) systems, we have attempted for the first time to determine the shear strength of interfaces in such systems by application of the Arcan *et al.* [5] method for testing material properties under uniform stress state fields. The test was previously applied to study interlaminar shear properties of composite materials [6] or other anisotropic materials [7, 8], as well as to study fracture mechanics of isotropic materials [9, 10].

A specially designed test specimen to be used with the loading fixture inducing a state of uniform plane stress in the critical section – the interface – was developed [11, 12] and has been used throughout this work. The advantages of this new test specimen and of its preparation procedure lie in the fact that it avoids specimen deformation or direct contact of coatings with a bonding agent and, on the other hand,

0022–2461/90 $03.00 + .12

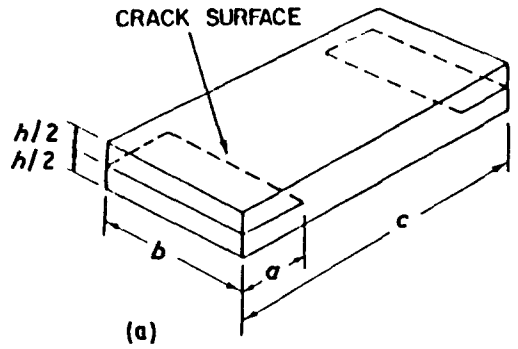

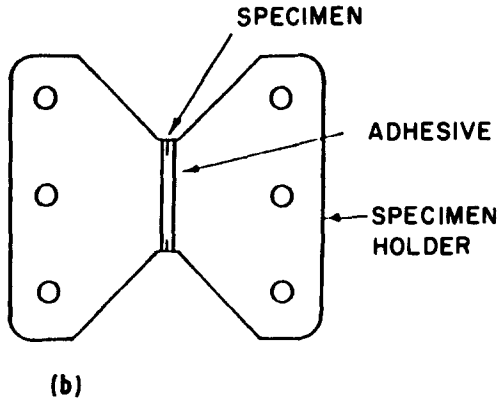

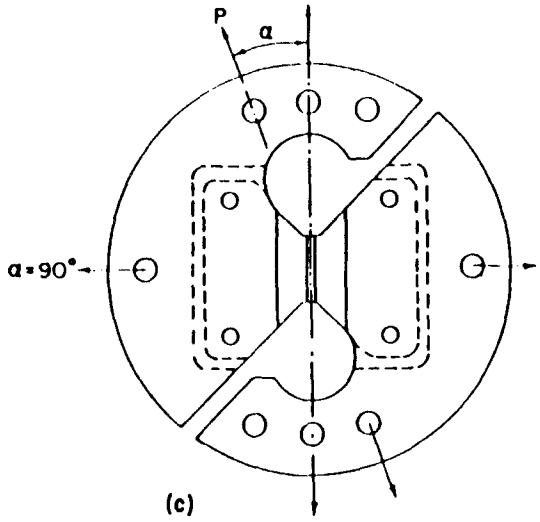

Figure 1 (a) the crosslinked specimen geometry (a = 4, 8, 12 mm, b = 19 mm, c = 38 mm, h = 2.5 mm); (b) the butterfly shaped holder and (c) the loading system showing pure shear and mixed mode loading.

in the fact that geometrical symmetry is basic for shear test.

This paper reports on a preliminary assessment of the Arcan *et al.* test (in pure shear mode only) in the case of adhesive bonding of a fast cure thermosetting powder coating (L) used for corrosion protection of a cold-rolled steel (S) surface.

2. Materials

Cold-rolled steel in sheet form, about 1.25 mm thick, manufactured by three suppliers was used throughout this work as the metallic substrate material for phosphating. The three steels were designated as S1, S2 and S3. The material underwent subsequent phosphating stages of the production plant (Pachmas, En Hahoresh, Israel) which developed this procedure as a pretreatment for steel surface before painting. The resulting iron phosphate layer (P) was typically about 0.4 μm thick (0.35 g m^{-2}). Further treatments of these sheets were carried out on a laboratory scale. A fast cure (thermosetting epoxy resin–phenolic hardener) powder (Libert, Ghent, Belgium) was used for coating. Powder was applied by electrostatic spraying using a Nortson powder coating gun operating at 60 kV, which offers good reproducibility.

3. The specimen

In order to investigate the interface true adhesion strength in the (SL) and (SPL) systems, a specially designed specimen and cross-linking preparation procedure were developed to model the complex fracture of the interface. Several geometries were considered and finally a symmetrical test specimen to enable proper mechanical behaviour under shear (initiation of fracture, and uniform plane stress loading in the interface plane). The geometry of the cross linked specimen for testing and of its loading system is presented schematically in Fig. 1.

The preparation procedure was pursued in the sequence: coupons of 1.5″ × 0.75″ (38 mm × 19 mm) were cut from the above cold-rolled steel panels (S1, S2 and S3) and iron-phosphated cold-rolled steel (S1P, S2P and S3P), respectively. The coupons were cleaned ultrasonically and rinsed several times with detergent, distilled water, and trichloroethylene (TCE), and then air-dried. To initiate a crack in the specimen, a thin (~ 70 μm) Teflon strip was inserted before the thermosetting powder film (70 to 80 μm thickness) was electrostatically sprayed over the coupons and then subjected to 120° C for 5 min. At

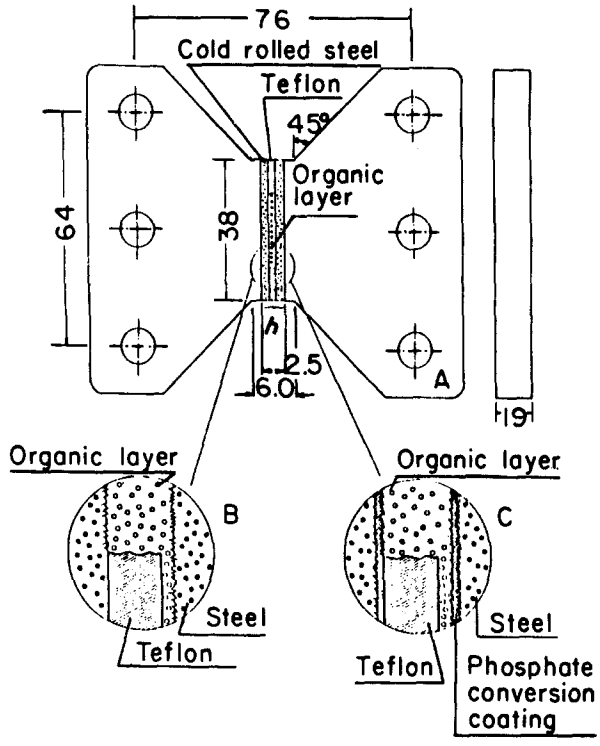

Figure 2 The crosslinked specimen and mounting for pure shear testing: (A) specimen mounted in holder; (B) detail of SL specimen; (C) detail of SPL specimen.

this temperature the coated powder just melted or fused, with the melted individual powder particles coalescing into a continuous layer. At this stage two lacquered specimens of the same base material, one of them bearing the Teflon strips to produce crack initiation, were stuck together and bonded by crosslinking during stoving for an additional 15 min at various experimental temperatures. Ranges were selected from 180 to 190° C for the underaged interval of temperatures, to 200 to 210° C in the region of known good adhesion and to 220 to 240° C for the overaged temperatures. During this stage a limited and constant pressure was applied until the thickness (70 to 90 μm) of the lacquer layer was achieved. All steps in preparation of the specimen were kept constant throughout the work in order to acquire reproducible specimens. The configuration was 10 to 30% symmetrically cracked, allowing a minimum area of 240 mm^2 coating to be tested. Details of the crosslinked specimen geometry are given in Fig. 2.

4. Mechanics of the test

The testing system is presented in Figs 1b and 1c. As mentioned elsewhere [5, 6, 8] and shown schematically in the Fig. 3, the shear stresses (equivalent to 45° directed principal stresses $\sigma_1 = -\sigma_2$) are pure and uniformly distributed along the whole section. Being a stiff adherent specimen, the present system may be considered as made of near two infinitely rigid strips and the crosslinked lacquer an adhesive layer. In such a case, the layer is submitted to the above mentioned uniform state of stress with subsequent 45° cracks (Fig. 3) perpendicular to σ_1 if the lacquer is brittle.

Crack propagation, when approaching the interface with the metallic substrate, will obviously be parallel to that interface.

5. Ultimate shear stress determination

Ultimate shear stress values on crosslinked specimens were determined after bonding the specimen to an intermediate holder (butterfly shaped, as shown in Fig. 1b). Bonding was achieved by glueing with a strong Araldite AV138M/Hardener HV998 (Ciba-Geigy). Previous sand blasting of surfaces and 30 h cure at 70° C were also required. A special device was used during curing to prevent misalignment while excess glue or squeeze out was removed carefully to ensure proper positioning of the specimen.

The crosslinked specimen glued to the intermediate holder was mounted in the circular loading test frame with antisymmetric cutouts (Fig. 1c) and attached with two symmetric pins on each side in the Instron machine. Crosshead speed was 0.01 mm min^{-1}. Displacement and load were recorded until failure occurred. From the experimentally measured critical load at which the interface failed, the ultimate shear stress values (USS N mm^{-2}) were calculated.

It should be emphasized that by loading the specimen to its circular loading frame in different rotated positions in the testing machine (Fig. 1c), both pure shear state (for $\alpha = 0°$) and mixed modes may be induced in the specimen; these characteristics of the loading system offer a large range of versatility to the testing process.

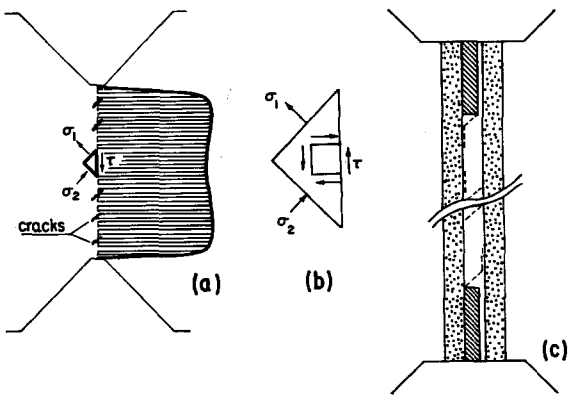

Figure 3 Mechanics of shear fracture: (a) pure shear diagram; (b) details of stresses on elementary volume; (c) crack development in pure shear mode.

6. Fracture surface analysis

Upon completion of the mechanical tests the two matting parts of the fractured specimens were examined using optical stereo microscopy, SEM fracture surface morphology analysis, as well as X-ray microanalysis. In order to enhance image contrast and to avoid charge effects, fractured areas were previously coated with gold and/or carbon films. The analysis process used a scanning electron microscope (SEM) JEOL and a Cambridge Stereoscan 180 equipped with an energy dispersive spectrometer (EDS) Proxan III interfaced to a PC XT computer.

X-ray analysis identified different fracturing stages, thus contributing to failure analysis (fracture surface appearance, location of crack initiation and the associated fracture micromechanisms).

7. Results and discussion

7.1. Shear test results

7.1.1. Testing parameters

In order to present critical stress values resulting from the failure test and the calculated stress intensity factor, one should first select and define the basic geometry and mechanical data (see Figs 1 and 3):

(i) inital crack length $a = 4$, 8 and 12 mm

(ii) section total nominal area $A_n = b \times c = 722$ mm^2

(iii) critical load P_c

(iv) nominal ultimate shear stress value $(USS)_n$

$$\tau_n = P_c/A_n$$

(v) net ultimate shear stress values $(USS)_{net}$

$$\tau_{net} = P_c/A_{net}$$

(vi) critical stress intensity factor (SIF), Mode II [13, 14];

$$K_{IIC} = f_{II}\tau_{net}[h/(1 - \nu)]^{1/2}$$

where: f_{II} are the correction factor values for the stiff adherent specimen with symmetric crack length up to 30%, τ_{net} the $(USS)_{net}$ values, h the lacquer thickness (0.07 mm) and ν, the Poisson coefficient (0.34).

7.1.2. Test results

The shear tests were designed to measure the critical Stress Intensity Factors as well as the nominal and the net strength values of interfaces of lacquered cold-rolled steel specimens. The test results are the experimentally measured critical stress values at which the adhesion of the organic coating on cold-rolled steel base material failed.

We selected on purpose the experimental parameters of the specimen in order to determine whether the test can indeed discern subtle variations influencing adhesion. The parameters chosen were: type of cold-rolled steel base material, a standard iron phosphate pretreatment of 0.35 g m^{-2} and three stoving temperatures (180, 200 and 220° C).

An experimental determination of the correction factors f_{II} provided the following values

Relative crack length	10%	20%	30%
f_{II}	1.02	1.10	1.35

Using these values, the critical SIF (K_{II}) could be obtained for every considered case (type of steel and stoving temperature). Table I presents both the USS net values and the SIF (K_{II}) values obtained for a relative crack length of 30%.

Due to the fact that the values of K_{IIC} were obtained from the USS_{net} values multiplied by the constant $f_{II}\sqrt{h}/(1-\nu)^{1/2}$, we present, in the resulting diagrams, only these last values.

Figs 4 and 5 show shear test results. Each data point represents the mean value and standard deviation of a minimum of 12 test specimens. The data presented in Fig. 4 show that shear strength values of 30 to 40 N mm^{-2} were obtained for S1 and S3 specimens which were not iron-phosphate-pretreated before coating. Specimens given an iron phosphate pretreatment exhibited shear strength values ranging from 40 to 50 N mm^{-2}.

The effect of lacquer stoving temperatures on the initial strength of the iron-phosphated and iron-phosphate-free interface systems is also shown in Figs 4a and 4b for S1 and S3 cold-rolled steel, respectively. Lower shear strength $(USS)_{net}$ values were obtained when lacquer stoving was at 180 than at 220° C. These figures indicate, as expected, that higher stoving temperatures promote higher $(USS)_{net}$ values, suggesting better adhesion.

Based on the shear failure test results obtained,

TABLE I Basic mode II mechanical properties of lacquer-steel specimens

Specimen	$(USS)_{net}$ (N mm^{-2})	K_{IIC} (N $mm^{-3/2}$)
S1PL180	41.5 ± 1.8	17.9
S3PL180	38.6 ± 2.2	16.6
S1PL200	46.4 ± 3.9	20.0
S2PL200	35.5 ± 3.4	15.3
S3PL200	44.8 ± 0.6	19.4
S1PL220	50.2 ± 2.1	21.7
S3PL220	46.8 ± 0.2	20.2

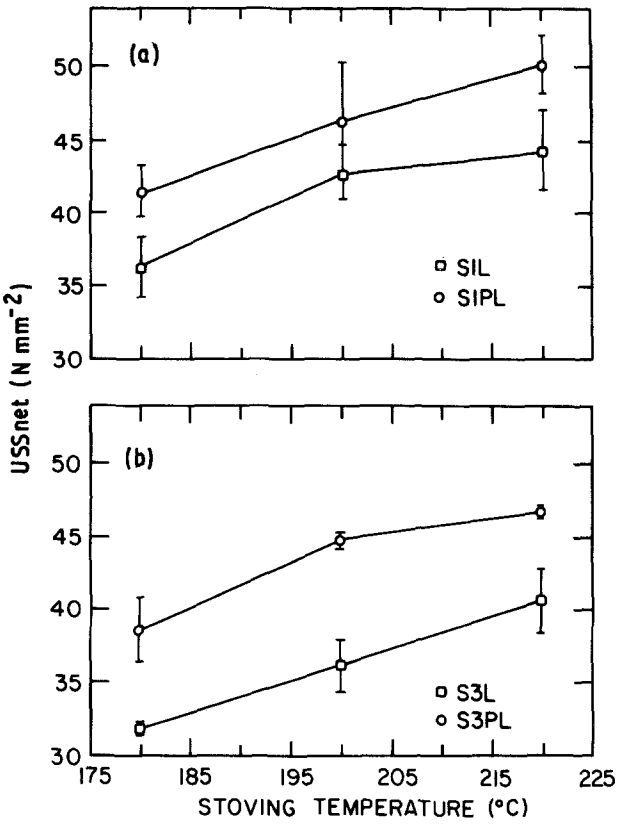

Figure 4 Adhesion characteristics: effect of iron phosphate treatment on $USS_{(net)}$ values in the shear test. (a) S1 steel substratum; (□ S1L, ○ S1PL) (b) S3 steel substratum (□ S3L, ○ S3PL).

we tried to compare and evaluate the quality of the three cold-rolled steel base materials (S1, S2, S3) for adhesion – after iron phosphating. The results (Fig. 5) indicate that higher shear strengths were obtained with specimens S1P than with S3P and S2P, revealing an adhesion strength rating of S1P > S3P > S2P.

The differences in $(USS)_{net}$ values obtained were related with the surface morphology of iron phosphate layer as it forms during the phosphating process. Previous TEM studies on the same iron phosphate layers (S1P, S2P, S3P) [15] provided experimental

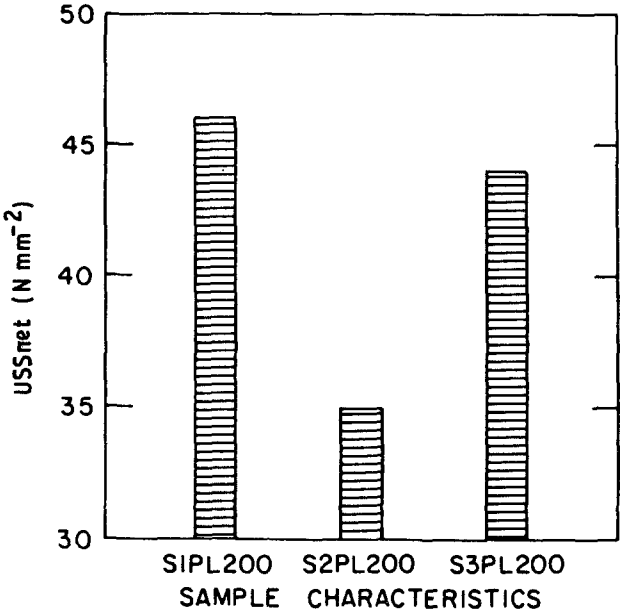

Figure 5 Adhesion characteristics: effect of type of cold-rolled steel substratum on $(USS)_{net}$ values in the shear test.

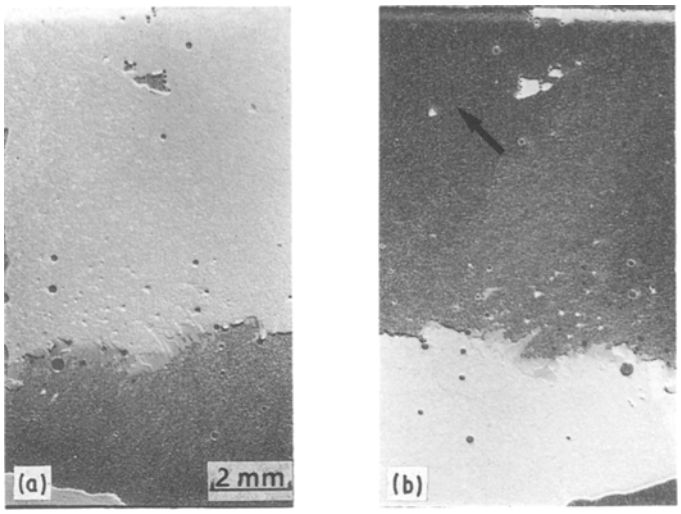

Figure 6 Optical micrographs revealing typical mating fracture surfaces of shear failed SL specimens. Note fracture start at crack origin sites in the interface region: (a) lacquer side; (b) metal side.

evidence of the interesting differences in their surface morphology, while revealing similar microstructures, essentially of $Fe_3(PO_4)_2 \cdot 4H_2O$. It was suggested that variations in morphology were due to the respective steel surface conditions resulting from differences in annealing and cold-rolled stages during steel manufacturing.

The structural and morphological aspects which can affect lacquer adhesion properties generally are grain size, orientation, stress and strain, texture, defects, and whether the layer grew epitaxially. Layers deposited on S1P substrate showed the presence of amorphous grains of $Fe_3(PO_4)_2 \cdot 4H_2O$ together with thin microsites of a mixture of iron oxides. The very fine surface morphology suggests numerous bond interlocking sites which could explain the higher $(USS)_{net}$ values (42 to 50 N mm^{-2}) obtained with these specimens.

In contrast, the lower $(USS)_{net}$ values ($\sim$ 35 N mm^{-2}) obtained with S2P specimens correlate well with the unusual microstructure of iron phosphate layer on the S2 substrate with its bimodal grain size distribution and localized epitaxial growth occurring on some particles giving rise to larger grains. Poor bond with

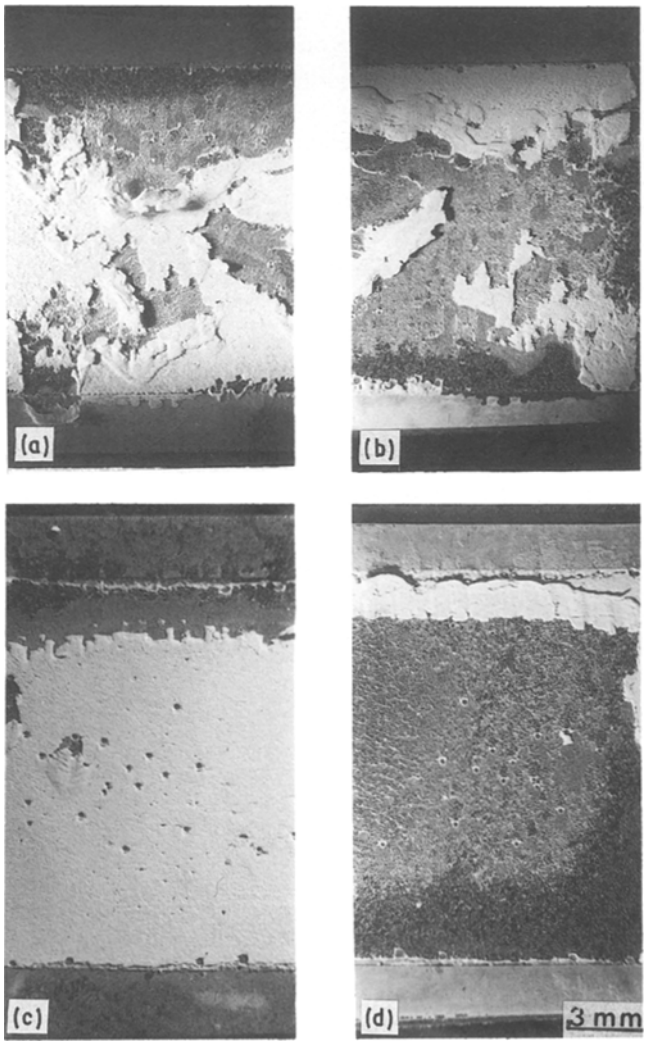

Figure 7 Optical micrographs revealing typical fracture mechanism transition in shear failed SPL specimens: (a) the lacquer side and (b) the mating metal side of the fracture showing strip-like initiation zones with flat appearances which develop into a zigzag pattern between the layers. Note conjugated layers on the fracture surfaces. (c) and (d) the mating fracture surfaces of another SPL shear failed specimen revealing the strip-like initiation zones and in (d) a thin film attached to the steel support suggesting crack propagation mainly in an "interphase"-like region.

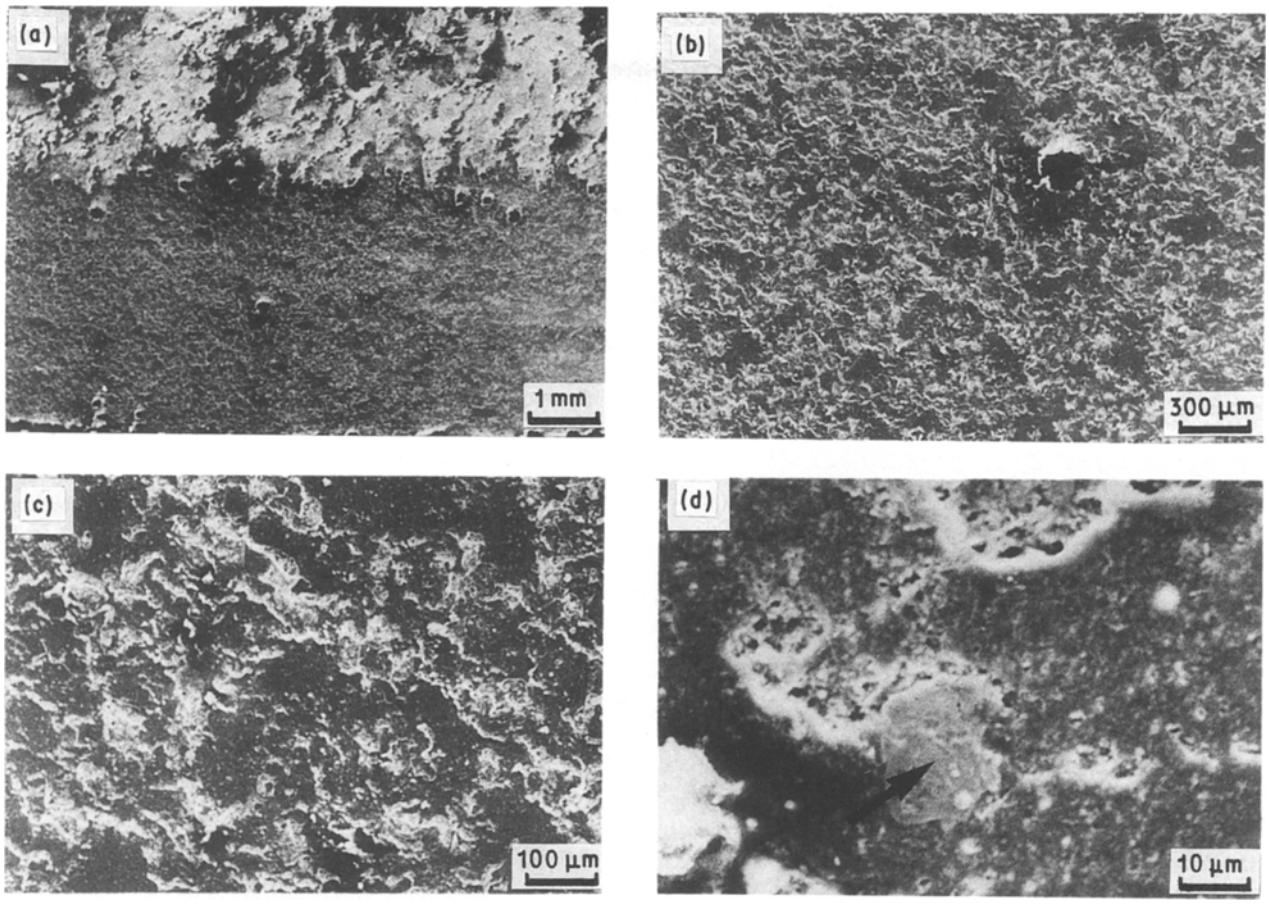

Figure 8 SEM micrographs of typical fracture surfaces of shear failed SPL specimens. Note in (a) and (b) the starting strip-like zone with alternating interlocks with flat appearances suggesting the interface plan. At higher magnification (c) and (d) particles in the dark, flat areas were identified as phosphate compounds by EDS analysis.

the lacquer layer should be expected for such a smooth surface. The morphology of layers deposited on the S3 substrate showed a homogeneous distribution of round-shaped grains, slightly larger than those on S1 substrate, corresponding well with the $(USS)_{net}$ values (39–47 N mm^{-2}) obtained in the actual shear failure test.

7.2. Fractography of the pure shear tested specimen

Shear-failed specimens were examined on mating surfaces to reveal fracture mechanism. Figs. 6 and 7 are a series of typical optical micrographs of SL and SPL fracture interfaces. Fig. 6 is an overall view of the SL system fracture resulting from the shear test, showing the two mating surfaces. These micrographs show that the fracture starts simultaneously at the two crack origin sites (the lower crack origin only visible in Figs 6a and 6b). The strips with a flat appearance present on both sides of the fracture sample, indicate that cracks start on opposite interfaces and propagate further mainly in the interface steel–lacquer (S–L)

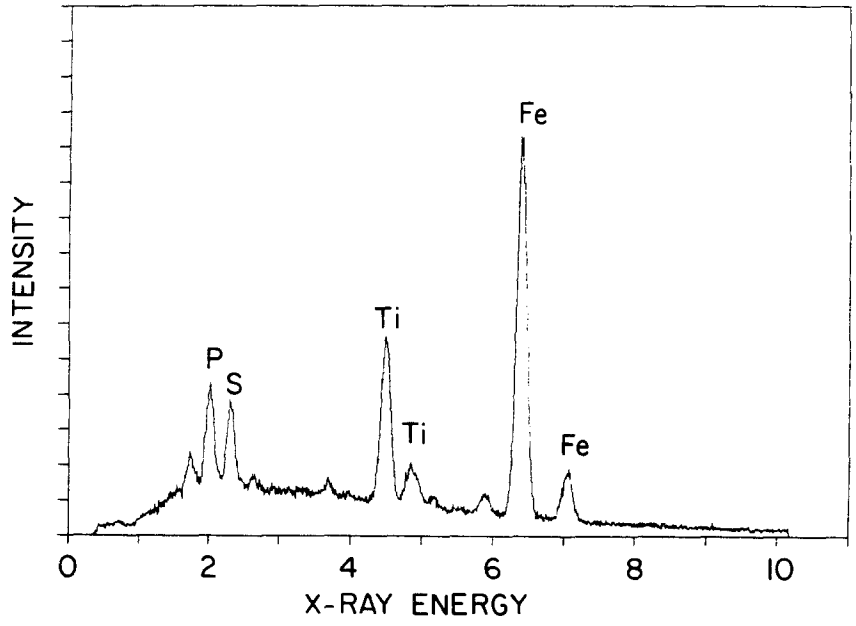

Figure 9 EDS analysis in interface area: elements of both the support (peaks of phosphorus and iron) and lacquer layer (sulphur and titanium) are present in the X-ray spectrum.

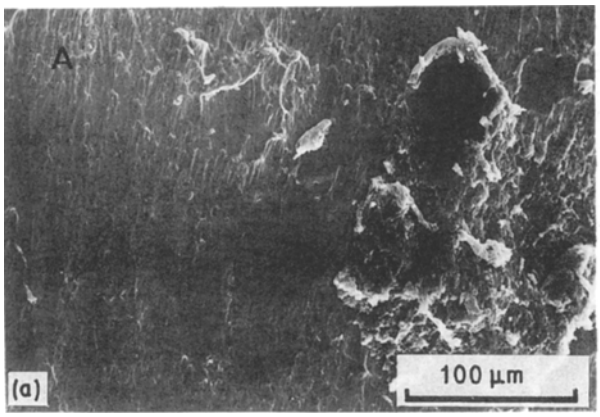

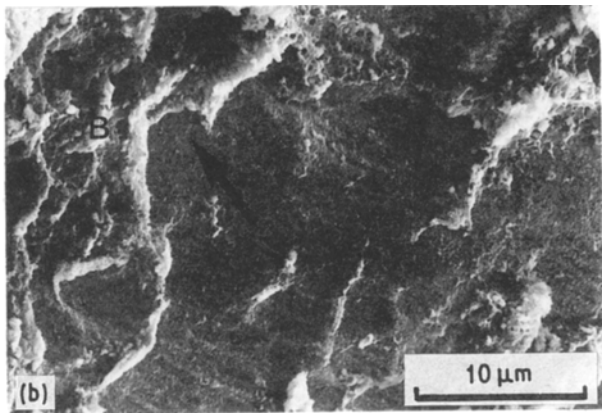

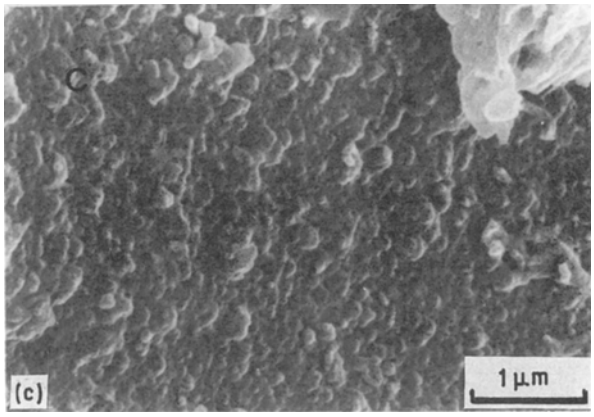

Figure 10 SEM micrograph of fracture surfaces tested in the shear mode: (a), interface S–L separation in an SL sample; (b), interface P–L in an SPL sample; (c), detail of (B) in the phosphate compound area.

region, with a few jumps through the lacquer bulk (see the dark area indicated by an arrow in Fig. 6b). This behaviour suggests that in this system the strength of the cohesive bond in the lacquer layer exceeds the interfacial bonding S–L. Typical $(USS)_{net}$ values obtained with this type of material were 30 to 40 N mm^{-2}.

Fig. 7 presents optical micrographs showing characteristic surface fracture patterns resulting from SPL system shear tests. Examination of the fracture interfaces on mating surfaces revealed a crack start behaviour – initiation from both crack origins of the specimen – similar to that obtained with the SL system and certainly resulting from the pure shear state induced during the test. The two starting strip-like initiation zones propagate simultaneously across the interface, with subsequent crack zigzags crossing the lacquer bulk several times and leaving conjugated layers on the fracture surfaces. Sometimes a different failure pattern was obtained, as shown in Figs. 7c and 7d. Here, a thin lacquer layer – the remains of some lacquer whiskers (visible at low magnification as a homogeneous film) – could be observed attached to the steel support (see Fig. 7d), the metal side of the fracture), suggesting that cracks progress mainly in an "interphase"-like region [2]. These results correlate well with the higher $(USS)_{net}$ (40 to 50 N mm^{-2}) values obtained with the SPL system (see also Fig. 4).

Fig. 8 are SEM micrographs showing, at higher magnification, details of the characteristic SPL system fracture pattern after shear failure. Here, also, we can see how crack starts in a strip-like zone (Fig. 8a), advancing about 2 to 4 mm in the interface level, and then entering the lacquer bulk. In Figs 8b and 8c, at higher magnification, one can distinguish interlocked dark islands surrounded by areas with plastic deformations. The flat regions (dark islands) indicate a fracture separation of two phases in the interface P–L, suggesting that bonds between the phosphate film and the lacquer layer were weaker in those islands than in the surrounding areas, which failed in the lacquer bulk. The assumption of interface failure in these islands was supported by the energy dispersive spectrometry (EDS) investigation of fracture surfaces. Inclusions on the lacquer (arrow in Fig. 8d) were analysed by EDS and components from both metal support (phosphorus and iron) and lacquer layer (sulphur and titanium) were detected (Fig. 9).

Figure 11 Optical micrograph showing typical pattern of pure shear failed interface. Note the characteristic shear generated microcracks network: (a), lacquer side; (b), metal side of an SPL fracture specimen.

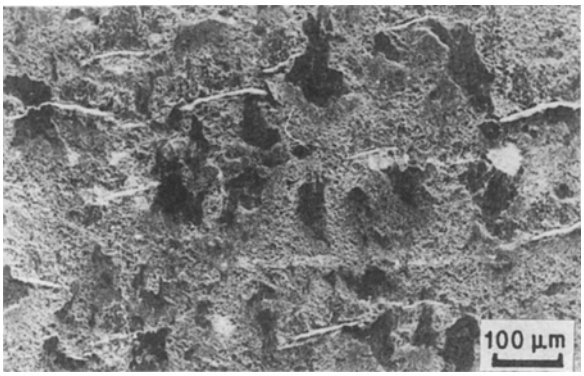

Figure 12 SEM micrographs showing microcracks and associate interlocked areas in an SPL shear failed specimen.

Fig. 10 presents SEM micrographs, showing the typical pattern of the fracture of the two systems, SL (Fig. 10a) and SPL (Figs. 10b and 10c). These micrographs reveal that in both systems the fracture separation occurs mainly at the interface level. While in the SL system the separation in the interface leaves the metal "smooth", suggesting weaker bounds, the fracture surface of the SPL system is rough, showing the remnants of some lacquer whiskers on the steel phosphate surface (see also Figs 7c and 7d), proving a stronger adhesion between phosphate and the lacquer layers. From these observations one may conclude that in SPL systems shear failure propagates mainly in an "interphase"-like region, containing the thin lacquer layer as part of the interface [2].

Examination of fracture interfaces on mating surfaces after testing revealed the presence of microcracks perpendicular to the crack propagation in most of the micrographs of SL and SPL fractured specimens. Fig. 11 is an optical micrograph showing microcracks on the mating fracture surfaces of the SPL system (a, microcracks on the failed lacquer surface; b, microcrack marks mirrored on the metal side). Fig. 12 is a SEM micrograph providing more details of the fracture pattern in the further propagation area. Microcracks and associated interlocked areas are easily visible in these patterns, suggesting that they form prior to shear failure. Fast and slow alternates of the crack growth in this system are related to interlocked areas as a consequence of strong bonds across the interface, together with local stress disturbances due to the formation of microcracks.

It is thought that these microcracks appear as a result of the specific loading process (see Fig. 3). We would like to emphasize here the similarities between the fracture pattern obtained after shear failure in this test, and the schematic sketch of the mechanics of shear failure presented in Fig. 3. The diagram of forces (Figs. 3a and 3b) shows that the state of stresses acting in the shear plane tends to create cracks at 45° in the specimen. A similar generated microcrack network was observed in most of the fracture pattern of SL and SPL systems tested, indicating fracture mechanism transitions characteristic of pure shear for both SL and SPL system.

In contrast, the fracture mode clearly was affected by differences existing in the interface structure and morphology of the two systems studied. In the case of SL system, fractures propagate mainly in the (smooth) interface, with stresses being more uniform and directed in the interface plane, where cohesion is weak. In the case of the SPL system, fractures propagate and change direction implying often that the direction and magnitude of the local applied stresses are variable and make fracture propagation more difficult. This behaviour correlates well with measurements of $(USS)_{net}$ in the test where higher values were obtained for SPL interfaces than for SL (see Fig. 4). These differences can be explained by the presence of an iron phosphate layer at the SPL interfaces.

These results are consistent with the previously mentioned observation [16, 17] that the fracture surface appearance depends on the material's microstructure as well as on the deformation mechanism which is active prior to fracture.

It should be emphasized that the combination of EDS analysis with macroscopic and SEM examinations of fracture surface, provided a useful insight into fracture phenomena and adhesion mechanisms, by detecting related components on the two sides of separation.

8. Conclusions

In the present work we considered adhesive failure as a fracture process and used the shear stress value at failure as quantitative information of the bond toughness along the interface.

An unusual specimen geometry was developed in order to enable symmetry of testing of a lacquered cold-rolled steel in a pure shear stress environment. These conditions were induced by adapting the Arcan test system. The superiority of this uncommon test specimen, apart from its symmetry – of utmost importance to this type of measurement – lies in the direct bonding by crosslinking. There is no contact between the coating to be tested and the bonding agent, which usually introduces additional unwanted stresses (deformation, chemical reaction, etc.).

Initiation of the fracture was produced intentionally and in a controlled way by two symmetric Teflon strips. The fracture, at least initially, was propagated in a plane of weakness for both LS and LPS interfaces.

Our main concern was directed to studies of the adhesion of two different non-soluble, immiscible, non-reacting material combinations. Three types of cold-rolled steels, as well as different lacquer curing temperatures, were considered. The shear test results were instrumental for selection of the right technology and basic materials for the entire process.

The fractographic and EDS analyses played an important role in leading to our understanding of the adhesion phenomena and in selecting the right specimen.

Acknowledgements

This research was supported by a grant from the Chief Scientist of the Israel Ministry of Commerce and Industry. We would like to thank Mr O. Rabina and Mrs Mazal Bery (Pachmas) for producing the samples.

References

1. K. L. MITTAL, ASTM STP 640 (American Society for Testing and Materials, Philadelphia, 1978) p. 5.
2. R. J. GOOD, ASTM STP 640 (American Society for Testing and Materials, Philadelphia, 1978) p. 18.
3. D. M. MATTOX, ASTM STP 640 (American Society for Testing and Materials, Philadelphia, 1978) p. 54.
4. J. J. BIKERMAN, ASTM STP 640 (American Society for Testing and Materials, Philadelphia, 1978) p. 30.
5. M. ARCAN, Z. HASHIN and A. VOLOSHIN, *Exp. Mech.* **18** (1978) 141.
6. L. ARCAN, M. ARCAN and I. M. DANIEL, ASTM STP 948 (American Society for Testing and Materials, Philadelphia, 1987) p. 41.
7. J. Y. LIU, *Wood and Fiber Sci.* **16** (1984) 567.
8. V. WEISSBERG and M. ARCAN, ASTM STP 981 (American Society for Testing and Materials, Philadelphia, 1988) p. 28.
9. L. BANKS-SILLS and M. ARCAN, ASTM STP 905 (American Society for Testing and Materials, Philadelphia, 1986) p. 347.
10. M. ARCAN and L. BANKS-SILLS, in Proceedings of the 7th International Conference on Experimental Stress Analysis, Haifa, April 1982, edited by A. A. Betser (Technion, Haifa, 1982), p. 187.
11. L. ARCAN *et al.*, *Ultramicroscopy* **23** (1987) 234.
12. Y. M. ARAVOT, M. Sc. Thesis, The Hebrew University of Jerusalem (1988).
13. A. N. GENT, *Rubber Chem. Technol.* **47** (1974) 202.
14. V. WEISSBERG and M. ARCAN, in "Experimental Stress Analysis", edited by H. Wieringa (Martinus-Nijhoff, Amsterdam, 1986) p. 255.
15. A. ALBU-YARON and O. RABINA, *Thin Solid Films* **162** (1988) 183.
16. R. W. HERTZBERG, in "Deformation and Fracture Mechanics of Engineering Materials" (John Wiley, New York, 1983).
17. R. W. HERTZBERG, ASTM STP 948 (American Society for Testing and Materials, Philadelphia, 1987) p. 5.

Received 21 February
and accepted 30 August 1989